RESEARCH ARTICLE

BATTERY ENERGY WILEY

Dual-functional ZnO/LiF layer protected lithium metal for stable Li$_{10}$GeP$_2$S$_{12}$-based all-solid-state lithium batteries

Xinshuang Chang[1,2] | Gaozhan Liu[1] | Ming Wu[1] | Mingyuan Chang[1] | Xiaolei Zhao[1] | George Z. Chen[3] | Kam Loon Fow[2,4] | Xiayin Yao[1]

[1]Ningbo Institute of Materials Technology and Engineering, Chinese Academy of Sciences, Ningbo, China

[2]Department of Chemical and Environmental Engineering, Faculty of Science and Engineering, University of Nottingham Ningbo China, Ningbo, China

[3]Department of Chemical and Environmental Engineering, Faculty of Engineering, University of Nottingham, University Park, Nottingham, UK

[4]Key Laboratory of Carbonaceous Wastes Processing and Process Intensification of Zhejiang Province, University of Nottingham Ningbo China, Ningbo, China

Correspondence
Kam Loon Fow, Department of Chemical and Environmental Engineering, Faculty of Science and Engineering, University of Nottingham Ningbo China, Ningbo 315100, China.
Email: kam-loon.fow@nottingham.edu.cn

Xiayin Yao, Ningbo Institute of Materials Technology and Engineering, Chinese Academy of Sciences, Ningbo 315201, China.
Email: yaoxy@nimte.ac.cn

Abstract

All-solid-state lithium battery has become one of the most promising secondary batteries due to their high energy density and excellent safety. However, the growth of lithium dendrites and side reactions between lithium metal and solid electrolytes hinder the practical application of all-solid-state lithium batteries. Herein, a dual-functional layer of ZnO and LiF is fabricated at the interface between lithium metal and Li$_{10}$GeP$_2$S$_{12}$ solid electrolyte by a magnetic sputtering technique. The ZnO/LiF dual-functional layer can suppress severe Li$_{10}$GeP$_2$S$_{12}$/lithium metal interface side reactions and has a high interface energy against lithium which can block the growth of lithium dendrites. The symmetric cell of Li@ZnO/LiF-Li$_{10}$GeP$_2$S$_{12}$-Li@ZnO/LiF demonstrates stable lithium plating/striping cycling for 2000 h with a small overpotential of 200 mV at 0.1 mA cm^{-2} and 0.1 mAh cm^{-2}. The full cell of Li@ZnO/LiF-Li$_{10}$GeP$_2$S$_{12}$-LiCoO$_2$@LiNbO$_3$ shows stable cycling stability for 500 cycles with a high reversible specific capacity of 80 mAh g^{-1} at 1.0 C.

KEYWORDS
all-solid-state batteries, interface modification, Li$_{10}$GeP$_2$S$_{12}$, lithium metal, ZnO/LiF dual-functional layer

1 | INTRODUCTION

Lithium-ion batteries with favorable energy density and long cycle life have been widely applied in portable electronic devices.[1–3] However, due to the theoretical capacity of commercially used oxide cathode and graphite anode, the energy density is approaching its limitation of around $300 \, Wh \, kg^{-1}$, which cannot meet the increasing demand of electric vehicles and large-scale energy storage systems.[4] This issue can be addressed by employing lithium metal anode instead of graphite benefiting from its low electrode potential ($-3.04 \, V$ vs. standard hydrogen electrode) and ultrahigh theoretical capacity of $3860 \, mAh \, g^{-1}$.[5,6] Another challenge is that lithium batteries using flammable organic liquid electrolytes would suffer serious safety problems when the short circuit happens due to the growth of lithium dendrite.

All-solid-state battery has become an alternative technology to overcome the safety hazard of lithium metal batteries due to their good mechanical and nonflammable properties.[7,8] Among all types of all-solid-state lithium batteries, sulfide solid electrolyte-based cells are the promising candidate for practical applications because the sulfide electrolytes possess high ionic conductivity, especially $Li_{10}GeP_2S_{12}$ shows an ionic conductivity of $12 \, mS \, cm^{-1}$.[9] Nevertheless, it is difficult to directly employ $Li_{10}GeP_2S_{12}$ in all-solid-state lithium batteries arising from severe interface reactions between lithium metal and $Li_{10}GeP_2S_{12}$.[10,11] Generally, an artificial protective layer fabricated at the interface can provide sufficient passivation between lithium metal and $Li_{10}GeP_2S_{12}$ solid electrolytes, such as Li-Ag,[12] Li-In,[13] Li_3PO_4,[14] or LiH_2PO_4.[15] However, these coating protection technologies only suppressed the side reactions between $Li_{10}GeP_2S_{12}$ and the lithium metal, lithium dendrites still grow in $Li_{10}GeP_2S_{12}$ even though the interface resistance is reduced. It is proposed that the interfacial layer with high interface energy can inhibit the growth of lithium dendrites. For example, LiF possesses a high interface energy of $73.27 \, eV \, Å \, m^{-2}$ against lithium metal, demonstrating high capability in lithium dendrite suppression.[8,16] Therefore, it is anticipated that a stable artificial layer with high interface energy against lithium could well address both side reaction and lithium dendrite growth and realize the application of the lithium metal in $Li_{10}GeP_2S_{12}$-based all-solid-state lithium batteries.

In this work, a ZnO/LiF dual protection layer is coated on the surface of the lithium metal by magnetic sputtering technique, aiming to stabilize the lithium/$Li_{10}GeP_2S_{12}$ interface and inhibit the growth of lithium dendrites. Compared with atomic layer deposition and chemical vapor deposition, magnetic sputtering shows the advantages of a high deposition rate, being environmentally friendly, easy to control, and high production efficiency, which can realize industrial production. During lithium plating, lithium deposits preferentially at the bottom of the lithiophilic ZnO, suppressing $Li_{10}GeP_2S_{12}$ reduction by lithium. And a lithiophobic layer of LiF with high interface energy suppresses lithium dendrite formation. The low electronic conductivity of LiF can further reduce the side reactions between lithium and $Li_{10}GeP_2S_{12}$. Li@ZnO/LiF-$Li_{10}GeP_2S_{12}$-Li@ZnO/LiF symmetric cell demonstrates stable lithium plating/striping cycling for 2000 h with a small overpotential of $200 \, mV$ at $0.1 \, mA \, cm^{-2}$ for 1 h. And the Li@ZnO/LiF-$Li_{10}GeP_2S_{12}$-$LiCoO_2$@$LiNbO_3$ full cell shows stable cycling stability for 500 cycles with a high reversible discharge capacity of $80 \, mAh \, g^{-1}$ at 1.0 C.

2 | EXPERIMENTAL SECTION

2.1 | Fabrication of Li@ZnO/LiF electrode

The Li@ZnO/LiF electrode was fabricated in three steps: First, lithium metal discs with thicknesses of 0.5 mm and diameter of 10 mm were obtained by punching the lithium metal ingot (Tianjin Zhongneng Lithium Industry Co., Ltd.). Subsequently, ZnO (Zhongnuo New Materials Technology Co., Ltd) was sputtered on the surface of lithium metal discs by magnetic sputtering (RH450) apparatus under 50 W, 0.5 Pa with a sample rotation speed of $20 \, r \, min^{-1}$ for 1 h to obtain the Li@ZnO electrode. Finally, LiF was sputtered on the surface of Li@ZnO under the same operation parameters for 6 h to get the Li@ZnO/LiF electrode. The thickness of the artificial membrane is controlled by the sputtering time. To characterize the thickness of the ZnO/LiF accurately, the ZnO and LiF were sputtered on the silicon surface under the same magnetic sputtering conditions. The magnetic sputtering equipment is equipped with a water-cooling system which is connected to the sample stage. The sample temperature can be controlled at 20°C during the sputtering process. All the procedures were performed in the glove box with an argon atmosphere.

2.2 | Characterization

Scanning electron microscope (SEM, Regulus-8230, Hitachi) and energy dispersive X-ray spectroscopy (EDX) were used to observe the surface morphology and element distribution of the Li@ZnO/LiF electrode.

X-ray photoelectron spectroscopy (XPS.AXIS ULTRA DLD) was used to identify the valence state of Zn, O, and F elements of the ZnO/LiF dual-functional layer.

2.3 | Cells assembling and electrochemical measurements

For the symmetric cells, $Li_{10}GeP_2S_{12}$ powder (150 mg) was compressed at 240 MPa to get a dense electrolyte pellet, Li@ZnO/LiF electrodes were then attached to both sides of the $Li_{10}GeP_2S_{12}$ pellet and further compressed at 360 MPa. For the full cells, the positive electrode was obtained by uniformly mixed $LiCoO_2@-LiNbO_3$ and $Li_{10}GeP_2S_{12}$ at a weight ratio of 70:30. Specifically, on one side of the $Li_{10}GeP_2S_{12}$ electrolyte

pellet, the positive material (3.0 mg) was dispersed evenly and densified at 120 MPa. Finally, the Li@ZnO/LiF disc was put on the other side of the electrolyte and pressed under 360 MPa. Both symmetric and full cells were tested on a battery test system (LAND CT-2001A, Wuhan Rambo Testing Equipment Co., Ltd.). The cell impedance tests were carried out on an electrochemical workstation (1470E) from 0.01 Hz to 1 MHz with an amplitude of 15 mV at 25°C.

3 | RESULT AND DISCUSSION

Fabrication procedures of Li@ZnO/LiF by the sputtering method are shown in Figure 1A. The ZnO and LiF layers are two independent and stable layers, and the
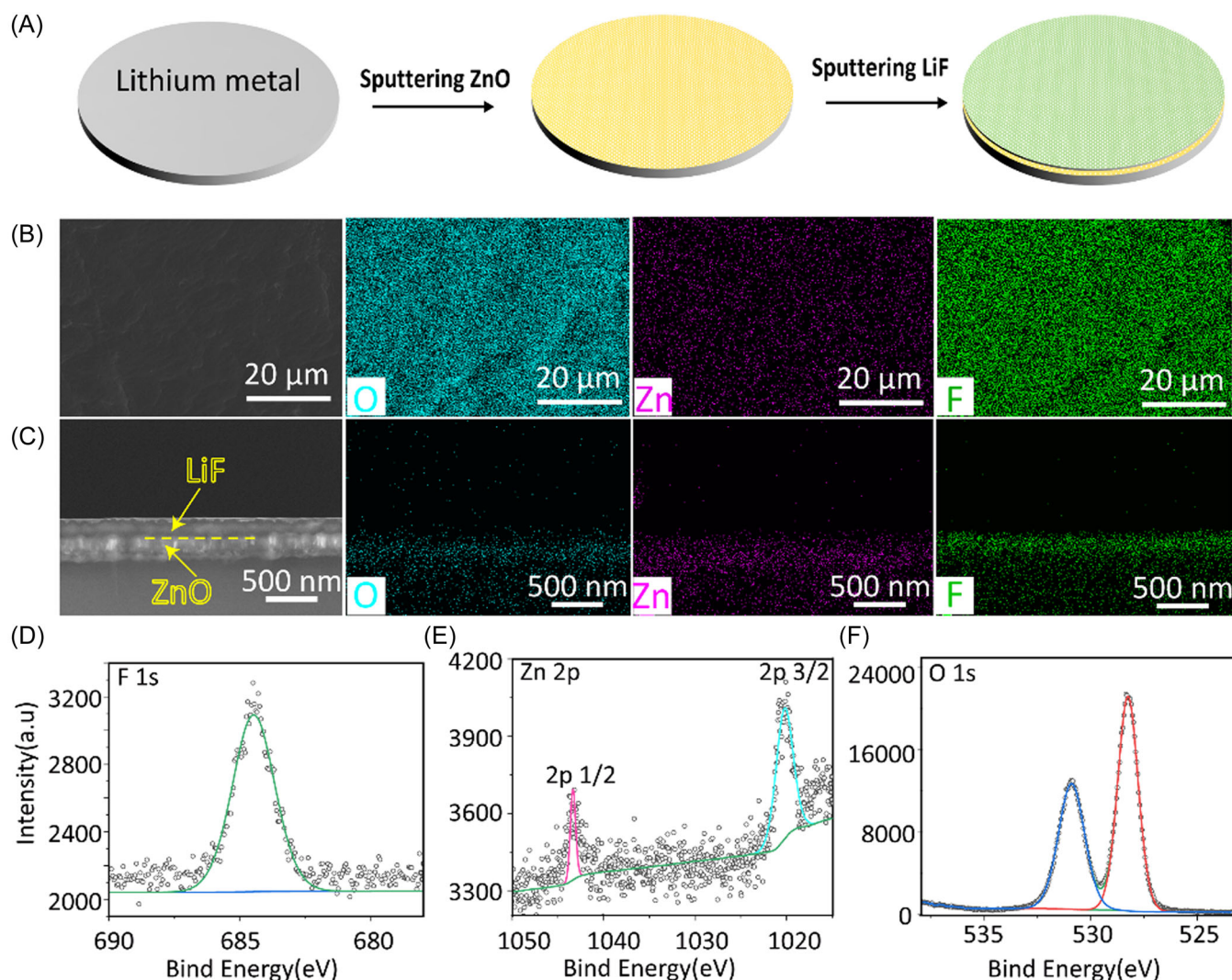

FIGURE 1 Fabrication strategy and the characterization of the Li@ZnO/LiF. (A) Schematic illustration of the fabrication processes of the Li@ZnO/LiF by the sputtering method. Scanning electron microscope (SEM) (B) top view and (C) cross-section images as well as the corresponding elemental mapping of Li@ZnO/LiF. The high-resolution X-ray photoelectron spectroscopy (XPS) pattern of (D) F 1s, (E) Zn 2p, and (F) O 1s for Li@ZnO/LiF.

lithiophilic ZnO could guide the lithium to deposit preferentially under the lithiophobic LiF layer away from $Li_{10}GeP_2S_{12}$. As shown in Figure 1B, Li@ZnO/LiF shows a smooth surface with O, Zn, and F elements well distributed on the surface of lithium metal. Moreover, the thickness of the ZnO and LiF protection layer can be identified by the cross-section view, showing 230 and 154 nm, respectively (Figure 1C). According to the thickness and the sputtering time, the average growth speed of the ZnO and LiF are 3.8 and 0.43 nm min^{-1}, respectively. Besides, the element types and electronic states on the surface of the lithium were characterized using XPS, and the XPS survey spectra proved the existence of F, Li, Zn, and O (Supporting Information: Figure S1). As shown in Figure 1D, the peak in the F 1s spectrum at 684.7 eV is corresponding to the LiF.[17] After etching the Li@ZnO/LiF during the XPS testing process, two peaks at 1043.4 and 1020.4 eV were found in Zn 2p spectrum, which is ascribed to the Zn 2p 3/2 and Zn 2p 1/2 (Figure 1E), confirming the existence of Zn^{2+} in ZnO.[18] The peaks in the O 1s spectrum (Figure 1F) at 530.9 eV are assigned to the O^{2-} in ZnO.[19] All these results proved that ZnO and LiF layers were well coated on the surface of the lithium.

The validity of the ZnO and LiF layers in protecting the $Li_{10}GeP_2S_{12}$/lithium interface was investigated, as shown in Figure 2. The symmetric cells with Li@ZnO/LiF, Li@ZnO, and Li electrodes were tested via the galvanostatic charge-discharge method at 0.1 mA cm^{-2} and 0.1 mAh cm^{-2} under 25°C. As shown in Figure 2A, LI-$Li_{10}GeP_2S_{12}$-Li only cycled for 450 h, and the cell overpotential drastically increased to 5000 mV and finally failed. Compared with bare lithium, the lithium stripping/plating overpotential decreased to 500 mV after coating the ZnO layer, and the symmetric cell could cycle for 2000 h, which could attribute to the reduced side reactions on the lithium/$Li_{10}GeP_2S_{12}$ interface. By further coating the LiF layer, the symmetric cell with Li@ZnO/LiF electrode stably cycled 2000 h, and the lithium plating/stripping overpotential decreased from 500 to 200 mV, indicating that ZnO and LiF could synergistically protect the lithium/$Li_{10}GeP_2S_{12}$ interface from side reactions and the formation of lithium dendrites.[8] With increasing areal capacity to 1.0 mAh cm^{-2} under 0.1 mA cm^{-2} (Figure 2B), the cyclic performance of the symmetric cells with Li@ZnO/LiF, Li@ZnO, and Li electrodes was further tested. The overpotential of symmetric cell with bare lithium reached 5000 mV after 320 h due to the severe side reaction, while it only increased to 1000 mV for Li@ZnO, and then reduced to 500 mV. It could reasonably speculate that the growth of lithium dendrite could lead to micro-short-circuit during the lithium plating/striping process. In addition,

the voltage plateaus of symmetric cells with Li and Li@ZnO increased suddenly indicating the uneven contact between the lithium and $Li_{10}GeP_2S_{12}$.[20] In contrast, for Li@ZnO/LiF-based symmetric cells, the voltage plateaus are flat and the overpotential maintains at 300 mV after 1000 h, which further proved that the LiF layer can block the development of the lithium dendrites and reduce the possibility of micro-short-circuit.

Figure 3 shows the rate capability of the Li@ZnO/LiF electrode. Under the current densities of 0.1, 0.25, 0.5, 1.0, and 0.1 mA cm^{-2}, the symmetric cell of Li@ZnO/LiF-$Li_{10}GeP_2S_{12}$-Li@ZnO/LiF shows small overpotential values of 15, 153, 564, 1431, 198 mV, respectively (Figure 3A). However, without ZnO/LiF layer, much larger overpotential values of 28, 258, 950, 5000, and 1931 mV were observed for the symmetric cell of Li-$Li_{10}GeP_2S_{12}$-Li under the same each current density. This result clearly confirms the superior stable lithium/$Li_{10}GeP_2S_{12}$ interface in the presence of Li@ZnO/LiF. Moreover, the rate capability of Li@ZnO/LiF-$Li_{10}GeP_2S_{12}$-$LiCoO_2$@$LiNbO_3$ and Li-$Li_{10}GeP_2S_{12}$-$LiCoO_2$@$LiNbO_3$ at different current densities from 0.1 C to 1.0 C were also presented (Figure 3B). The reversible discharge capacity for Li@ZnO/LiF are 115, 110, 100, and 80 mAh g^{-1} at 0.1, 0.2, 0.5, and 1.0C, respectively, and the discharge capacity was able to recover to 110 mAh g^{-1} at 0.1 C. On the contrary, the Li-$Li_{10}GeP_2S_{12}$-$LiCoO_2$@$LiNbO_3$ exhibits lower reversible discharge capacity under the corresponding current densities. Especially the discharge capacity is 41 mAh g^{-1} at 1.0 C, which is only half of that in Li@ZnO/LiF-$Li_{10}GeP_2S_{12}$-$LiCoO_2$@$LiNbO_3$ cell, demonstrating ZnO/LiF dual-functional protecting layer can effectively inhibit the side reaction on the lithium/$Li_{10}GeP_2S_{12}$ interface at high current densities.

The stability and dendrite suppression validity of the Li@ZnO/LiF electrode was further tested in all-solid-state batteries at 0.1 C, as shown in Figure 4 and Supporting Information: Figure S2. All the cells show initial discharge capacities of around 130 mAh g^{-1}. However, the Li-$Li_{10}GeP_2S_{12}$-$LiCoO_2$@$LiNbO_3$ cell shows a rapid capacity decay and failed after less than 30 cycles (Figure 4A). After coating the ZnO layer, a slow decay in discharge capacity was observed (Supporting Information: Figure S2a), but an unusual charge curve is found after 60 cycles (Figure S2b). The specific charge capacity gradually increased to 300 mAh g^{-1}, indicating a micro-short-circuit occurred in the cell due to lithium dendrites. By further coating the LiF layer, the cell with Li@ZnO/LiF shows a high initial discharge specific capacity of 126 mAh g^{-1} with capacity retention of 85% after 120 cycles (Figure 4B,C), exhibiting excellent lithium dendrite suppression. After five cycles of activation at 0.1 C, Li@ZnO/LiF-$Li_{10}GeP_2S_{12}$-$LiCoO_2$@$LiNbO_3$ exhibits a high specific

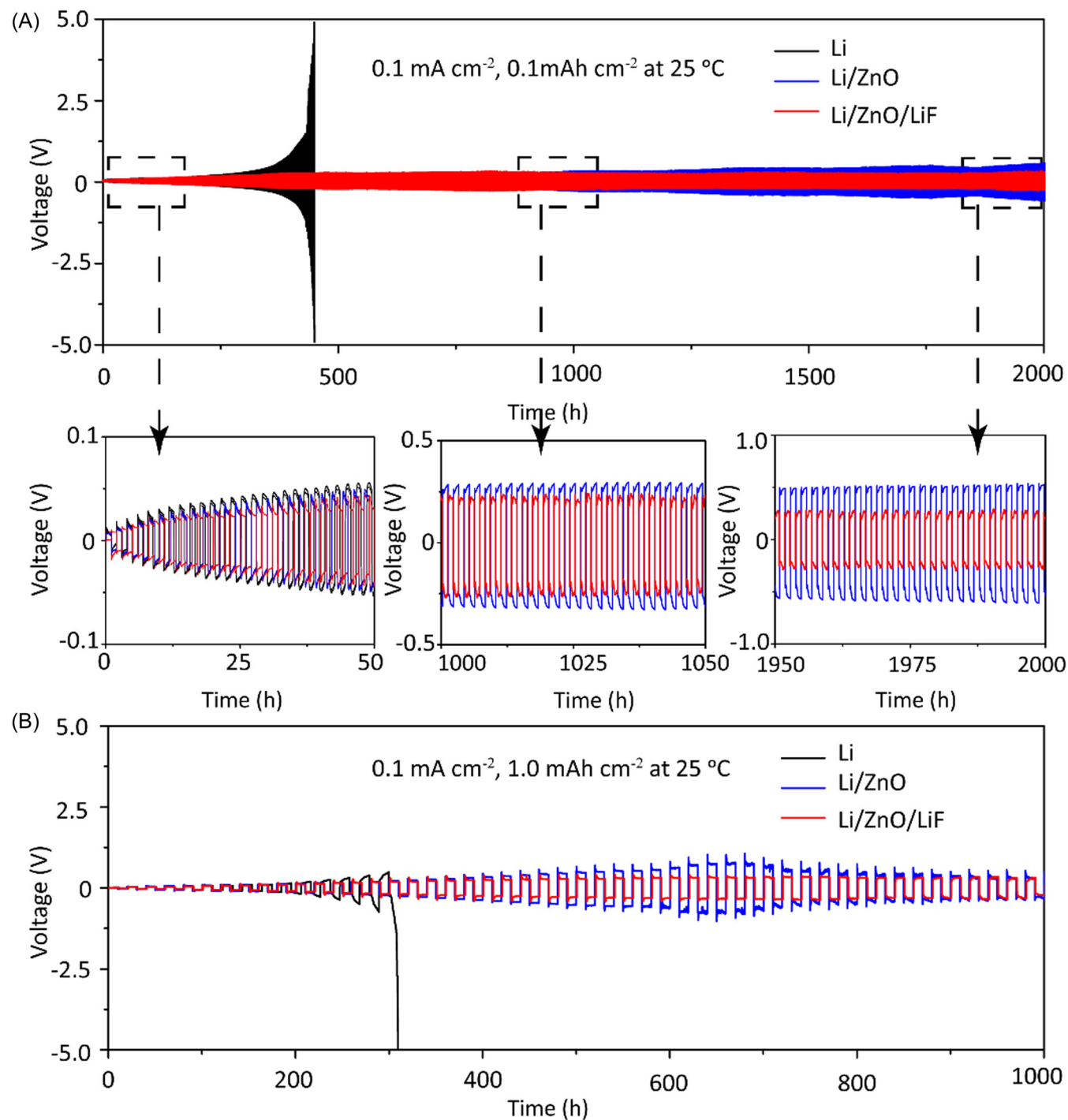**FIGURE 2** Lithium metal plating/striping cycling of $Li_{10}GeP_2S_{12}$-based symmetric cells with Li, Li@ZnO and Li@ZnO/LiF electrodes at $0.1\,mA\,cm^{-2}$ and (A) $0.1\,mAh\,cm^{-2}$, (B) $1.0\,mAh\,cm^{-2}$ under $25°C$

capacity of $80\,mAh\,g^{-1}$ with a capacity retention of 97% after 500 cycles at 1.0C (Figure 4D). The enhanced cyclic performance can be attributed to the well-controlled lithium stripping/plating behavior by the protection of the ZnO/LiF, which strongly proves the ZnO/LiF composite layer can achieve better electro-deposition of lithium even at a high current density.

To further understand the protective mechanism of the ZnO/LiF dual-functional layer on the lithium/$Li_{10}GeP_2S_{12}$ interface, the impedance of full cells with Li@ZnO/LiF and Li was conducted, as shown in Supporting Information: Figure S3. Before cycling, the Li@ZnO/LiF-$Li_{10}GeP_2S_{12}$-LiCoO$_2$@LiNbO$_3$ and Li-$Li_{10}GeP_2S_{12}$-LiCoO$_2$@LiNbO$_3$ show ohmic impedance
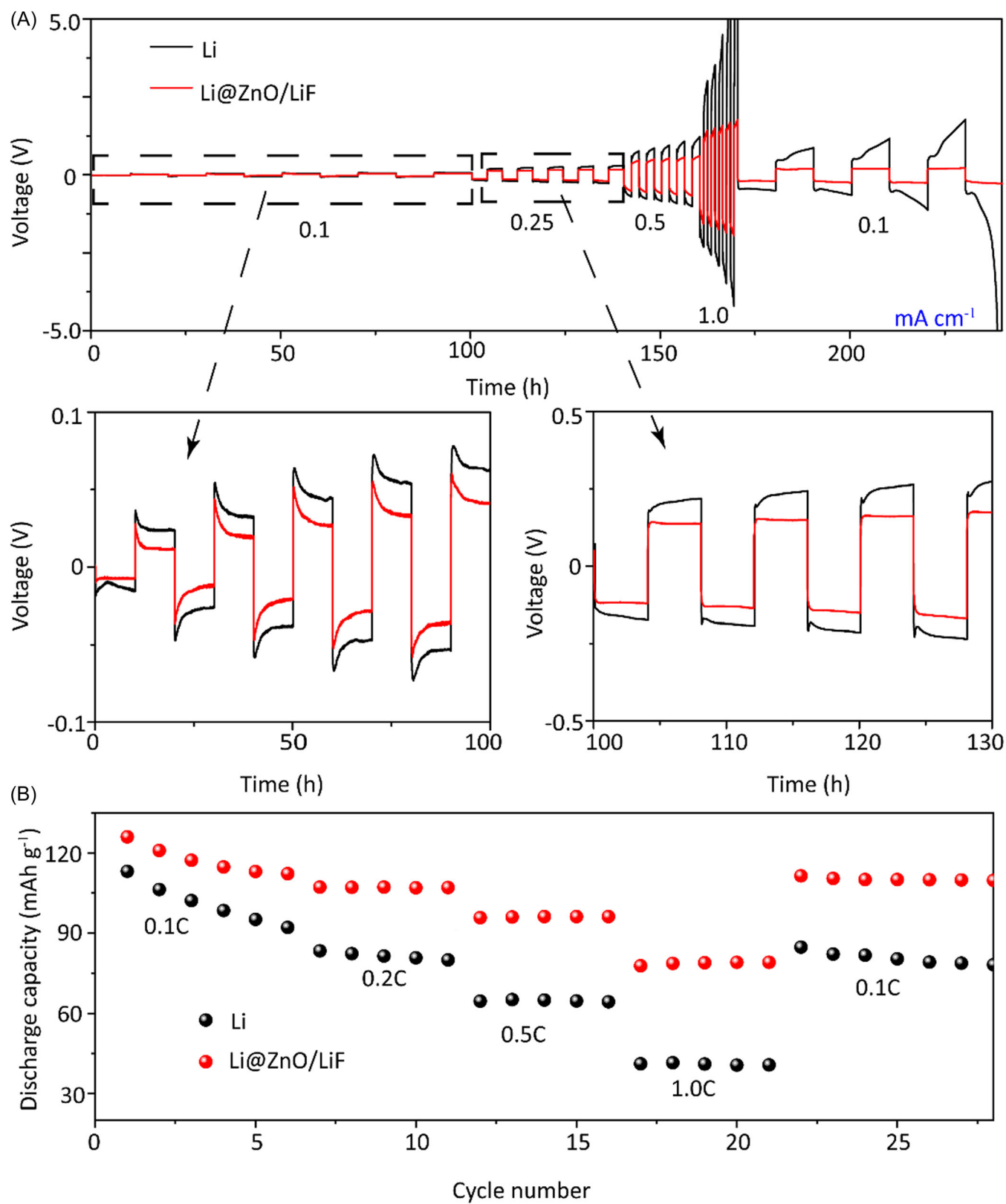
FIGURE 3 Rate capability of (A) the symmetric cells of Li@ZnO/LiF-Li$_{10}$GeP$_2$S$_{12}$-Li@ZnO/LiF, Li-Li$_{10}$GeP$_2$S$_{12}$-Li at 0.1, 0.25, 0.5, 1.0 mA cm^{-2}, (B) full cells of Li@ZnO/LiF-Li$_{10}$GeP$_2$S$_{12}$-LiCoO$_2$@LiNbO$_3$, Li-Li$_{10}$GeP$_2$S$_{12}$-LiCoO$_2$@LiNbO$_3$ cycled at 0.1, 0.2, 0.5, 1.0 under 25°C
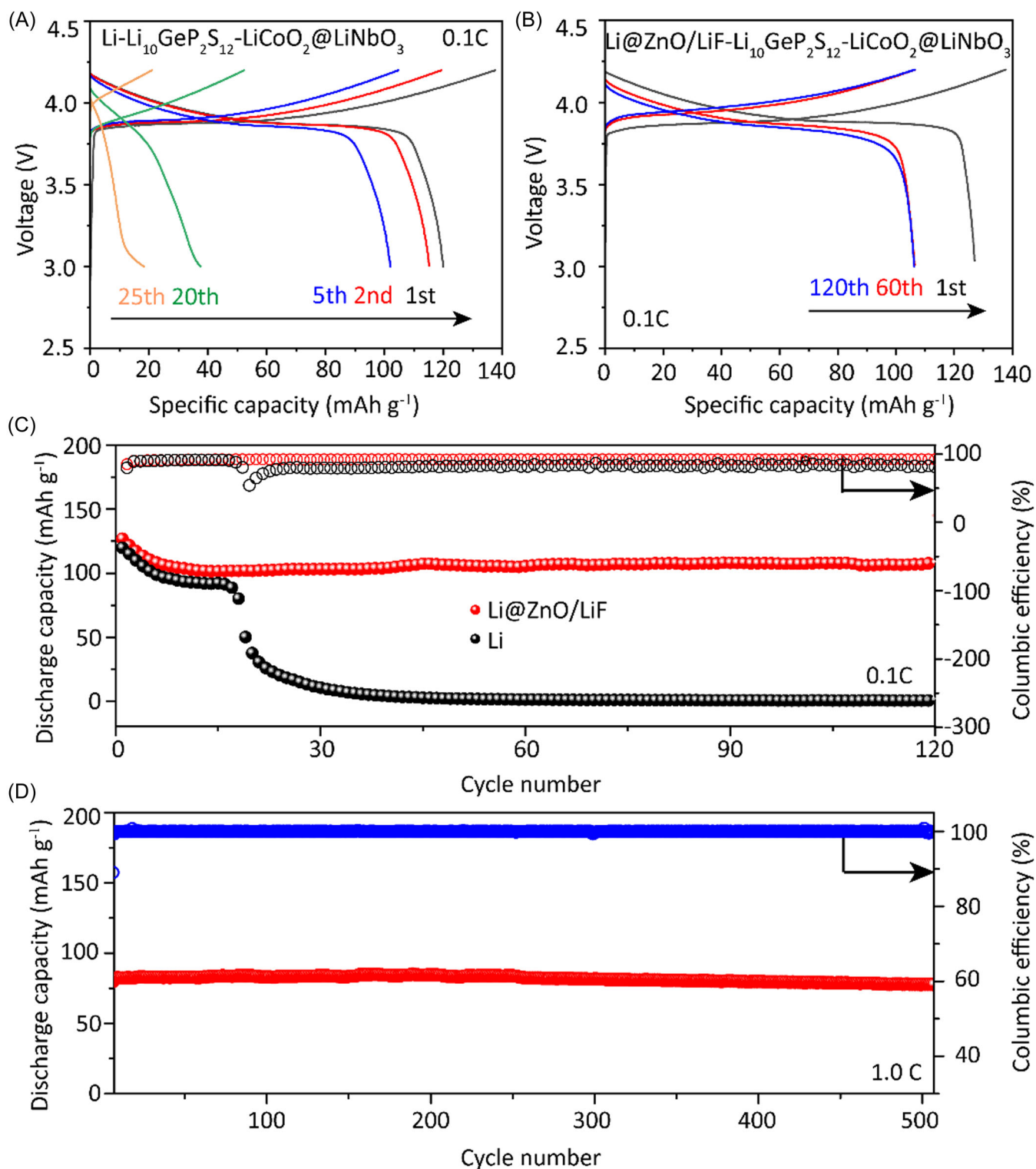
FIGURE 4 Cycle performance of full cells. Charge and discharge curves of (A) Li-$Li_{10}GeP_2S_{12}$-$LiCoO_2$@$LiNbO_3$ (B) Li@ZnO/LiF-$Li_{10}GeP_2S_{12}$-$LiCoO_2$@$LiNbO_3$, long cyclic performances of (C) Li@ZnO/LiF-$Li_{10}GeP_2S_{12}$-$LiCoO_2$@$LiNbO_3$, Li-$Li_{10}GeP_2S_{12}$-$LiCoO_2$@$LiNbO_3$ at 0.1 C, (D) Li@ZnO/LiF-$Li_{10}GeP_2S_{12}$-$LiCoO_2$@$LiNbO_3$ at 1.0 C under 25°C.

values of 60 and 48 Ω, respectively. After 120 cycles, the ohmic impedance value of the cell with bare lithium increased to 2800 Ω, which is much larger than that of Li@ZnO/LiF-$Li_{10}GeP_2S_{12}$-$LiCoO_2$@$LiNbO_3$ with 760 Ω,

indicating serious side reactions occurred between the $Li_{10}GeP_2S_{12}$ and lithium metal without the ZnO and LiF protection. The side reactions between lithium dendrite and $Li_{10}GeP_2S_{12}$ result in the formation of by-products

with a mixed ion-electron conductive layer at the lithium/ $Li_{10}GeP_2S_{12}$ interface, leading to a significant increase of ohmic impedance for Li-$Li_{10}GeP_2S_{12}$-LiCoO$_2$@LiNbO$_3$ cell. In contrast, the side reactions between the lithium metal and $Li_{10}GeP_2S_{12}$ and lithium dendrites were effectively suppressed by the synergistic effect of ZnO and LiF, resulting in a low ohmic impedance of Li@ZnO/LiF-$Li_{10}GeP_2S_{12}$-LiCoO$_2$@LiNbO$_3$.

Moreover, the morphology of cycled Li and Li@ZnO/LiF was analyzed by SEM. For bare lithium metal, a loose and rough surface with by-products was observed after depositing 1, 5, 10 mAh cm^{-2} lithium (Figure 5A–C). The by-products mainly include Li$_2$S, Li$_3$P, and Ge/Li-Ge alloy with poor lithium ion conductance and considerable electronic conductivity,[21]

leading to the uneven deposition of lithium metal and the growth of lithium dendrite. The dendrites will further increase the uneven contact of lithium metal with the $Li_{10}GeP_2S_{12}$ solid electrolyte, resulting in severe side reactions on the lithium/$Li_{10}GeP_2S_{12}$ interface with more by-products after the cycling. In contrast, the Li@ZnO/LiF electrode is dense, showing a suppressed dendrite and by-products stable interface between the lithium metal and $Li_{10}GeP_2S_{12}$ after depositing 1, 5, 10 mAh cm^{-2} lithium (Figure 5D–F). Figure 6 shows a schematic of the mechanism of the Li@ZnO/LiF dual-functional layer for protecting the lithium/$Li_{10}GeP_2S_{12}$ interface after deposition. During the lithium deposition process, the lithiophilic ZnO could guide lithium ions to deposit preferentially under
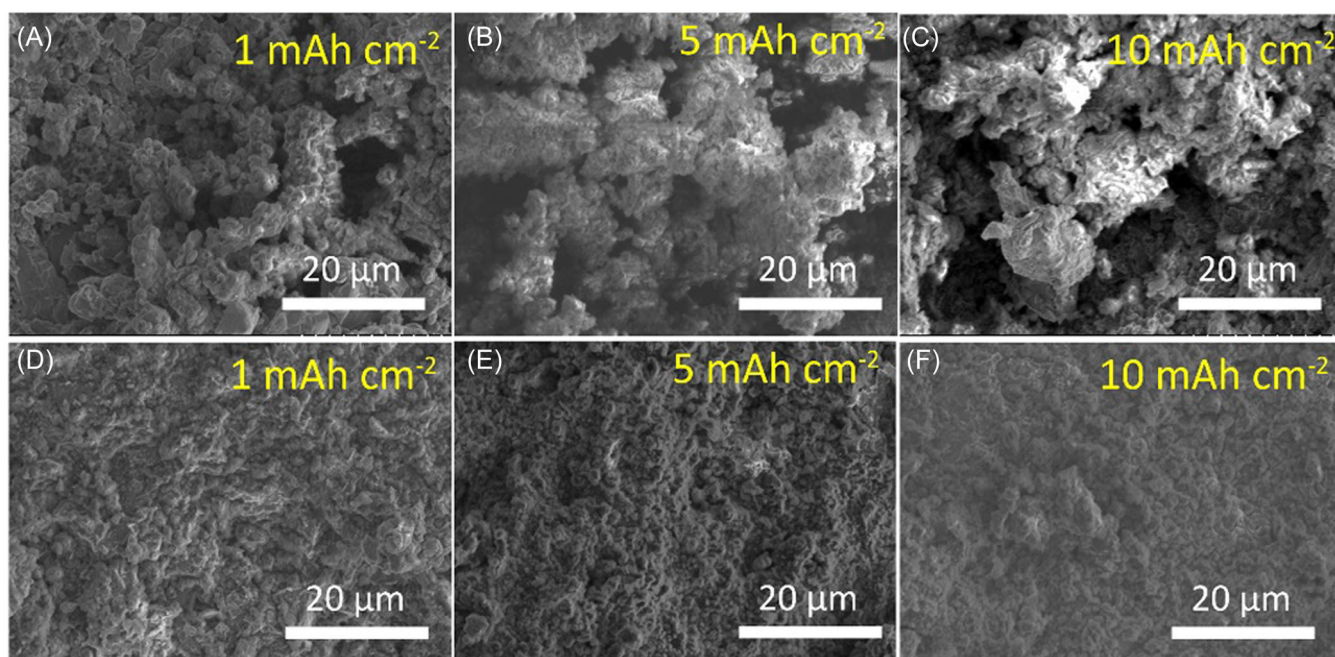

FIGURE 5 The surface morphology scanning electron microscope (SEM) images of (A–C) Li and (D–F) Li@ZnO/LiF deposited with 1, 5, 10 mAh cm^{-2} lithium metal
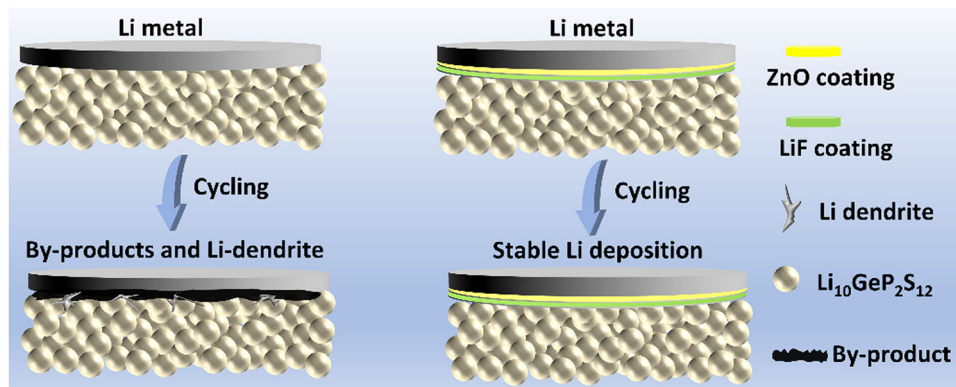

FIGURE 6 Proposed interfacial evolution of Li and Li@ZnO/LiF negative electrode with $Li_{10}GeP_2S_{12}$ after deposition

the LiF layer, which is away from the $Li_{10}GeP_2S_{12}$, consequently suppressing the reduction between lithium metal and solid electrolyte. The lithiophobic LiF with high interface energy and high lithium ion conductivity could further reduce the side reactions, and suppress the growth of the lithium dendrites during the lithium plating/striping process. As a result, the ZnO layer and LiF layer could synergistically lead to a stable interface with suppressed dendrites and by-products.

4 | CONCLUSION

To sum up, the stable dual-functional protecting layer of ZnO/LiF on the surface of lithium metal is fabricated by the magnetic sputtering technology, which can effectively protect the lithium/$Li_{10}GeP_2S_{12}$ interface and impede the growth of lithium dendrites. Consequently, the symmetric cell of Li@ZnO/LiF- $Li_{10}GeP_2S_{12}$- Li@ZnO/LiF demonstrates stable lithium plating/striping cycling for 2000 h with a small overpotential of 200 mV at 0.1 mA cm^{-2}. At 1.0C, the Li@ZnO/LiF-$Li_{10}GeP_2S_{12}$-LiCoO$_2$@LiNbO$_3$ full cell exhibits a high reversible discharge capacity of 80 mAh g^{-1} over 500 cycles. The synergistic effect of ZnO and LiF can simultaneously suppress the side reactions between the lithium metal and $Li_{10}GeP_2S_{12}$ as well as the growth of lithium dendrites, which provides a promising strategy for the application of lithium metal in $Li_{10}GeP_2S_{12}$-based all-solid-state lithium batteries.

CONFLICT OF INTEREST
The authors declare no conflict of interest.

DATA AVAILABILITY STATEMENT
The data that support the findings of this study are available from the corresponding author upon reasonable request.

ORCID
Xiayin Yao http://orcid.org/0000-0002-2224-4247

REFERENCES

1. Pang Y, Pan J, Yang J, Zheng S, Wang C. Electrolyte/electrode interfaces in all-solid-state lithium batteries: a review. *Electrochem Energy Rev.* 2021;4(2):169-193.
2. Yang C, Zhang L, Liu B, et al. Continuous plating/stripping behavior of solid-state lithium metal anode in a 3D ion-conductive framework. *Proc Natl Acad Sci USA.* 2018;115(15):3770-3775.
3. Wang C, Ma Y, Du X, Zhang H, Xu G, Cui G. A polysulfide radical anions scavenging binder achieves long-life lithium–sulfur batteries. *Battery Energy.* 2022;1:20220010.
4. Jiang J, Lu J, Ou Y, et al. Construction of a high-stability and low-nucleation-barrier Cu_3Sn alloy layer on carbon paper for dendrite-free Li metal deposition. *ACS Appl Mater Interfaces.* 2022;14(2):2930-2938.
5. Jiang J, Ou Y, Lu S, et al. In-situ construction of Li-Mg/LiF conductive layer to achieve an intimate lithium-garnet interface for all-solid-state Li metal battery. *Energy Storage Mater.* 2022;50:810-818.
6. Chen Y, Xu X, Gao L, et al. Two birds with one stone: using indium oxide surficial modification to tune inner helmholtz plane and regulate nucleation for dendrite-free lithium anode. *Small Methods.* 2022;6(5):2200113.
7. Zhao J, Zhao C, Zhu J, et al. Size-dependent chemomechanical failure of sulfide solid electrolyte particles during electrochemical reaction with lithium. *Nano Lett.* 2022;22(1):411-418.
8. Ji X, Hou S, Wang P, et al. Solid-state electrolyte design for lithium dendrite suppression. *Adv Mater.* 2020;32(46):2002741.
9. Chen B, Ju J, Ma J, et al. An insight into intrinsic interfacial properties between Li metals and $Li_{10}GeP_2S_{12}$ solid electrolytes. *Phys Chem Chem Phys.* 2017;19(46):31436-31442.
10. Xia S, Wu X, Zhang Z, Cui Y, Liu W. Practical challenges and future perspectives of all-solid-state lithium-metal. *Chem.* 2019;5(4):753-785.
11. Kamaya N, Homma K, Yamakawa Y, et al. A lithium superionic conductor. *Nat Mater.* 2011;10(9):682-686.
12. Li M, Zhou D, Wang C, et al. In situ formed Li-Ag alloy interface enables $Li_{10}GeP_2S_{12}$-based all-solid-state lithium batteries. *ACS Appl Mater Interfaces.* 2021;13(42):50076-50082.
13. Ma Y, Li L, Wang L, et al. A mixed modified layer formed in situ to protect and guide lithium plating/stripping behavior. *ACS Appl Mater Interfaces.* 2020;12(28):31411-31418.
14. Shi Y, Zhou D, Li M, et al. Surface engineered Li metal anode for all-solid-state lithium metal batteries with high capacity. *ChemElectroChem.* 2021;8(2):386-389.
15. Zhang Z, Chen S, Yang J, et al. Interface re-engineering of $Li_{10}GeP_2S_{12}$ electrolyte and lithium anode for all-solid-state lithium batteries with ultralong cycle life. *ACS Appl Mater Interfaces.* 2018;10(3):2556-2565.
16. Fan X, Ji X, Han F, et al. Fluorinated solid electrolyte interphase enables highly reversible solid-state Li metal battery. *Sci Adv.* 2018;4:1-10.
17. Zhao F, Sun Q, Yu C, et al. Ultrastable anode interface achieved by fluorinating electrolytes for all-solid-state Li metal batteries. *ACS Energy Lett.* 2020;5(4):1035-1043.
18. Xie F, Yang M, Song Z-Y, et al. Highly sensitive electrochemical detection of Hg(II) promoted by oxygen vacancies of

plasma-treated ZnO: XPS and DFT calculation analysis. *Electrochim Acta*. 2022;426:140757.

19. Chen T, Liu S-Y, Xie Q, Detavernier C, Meirhaeghe RL, Qu X-P. The effects of deposition temperature and ambient on the physical and electrical performance of DC-sputtered n-ZnO/p-Si heterojunction. *Appl Phys A*. 2009;98(2):357-365.

20. Ni S, Sheng J, Zhang C, et al. Dendrite-free lithium deposition and stripping regulated by aligned microchannels for stable lithium metal batteries. *Adv Funct Mater*. 2022;32(21):2200682.

21. Wang S, Fang R, Li Y, et al. Interfacial challenges for all-solid-state batteries based on sulfide solid electrolytes. *J Materiom*. 2021;7(2):209-218.

SUPPORTING INFORMATION

Additional supporting information can be found online in the Supporting Information section at the end of this article.

How to cite this article: Chang X, Liu G, Wu M, et al. Dual-functional ZnO/LiF layer protected lithium metal for stable $Li_{10}GeP_2S_{12}$-based all-solid-state lithium batteries. *Battery Energy*. 2022;20220051. doi:10.1002/bte2.20220051